Graphene Synthesis *via* Thermal Polymerization of Aromatic Quinone Molecules

Shigeki Kawai,[†,‡,*] Baran Eren,[†,§] Laurent Marot,[†] and Ernst Meyer[†]

[†]Department of Physics, University of Basel, Klingbergstrasse 82, 4056 Basel, Switzerland, [‡]PRESTO, Japan Science and Technology Agency, 4-1-8 Honcho, Kawaguchi, Japan, and [§]Material Sciences Division, Lawrence Berkeley National Laboratory, 1 Cyclotron Road, Berkeley, California 94720, United States

ABSTRACT Graphene was synthesized from pentacenequinone molecules on a Cu(111) surface using a three-step thermal treatment process: (1) self-assembly of a single layer molecular film at 190 °C, (2) formation of covalent bonding between adjacent molecules at intermediate temperatures, (3) thermal dehydrogenation and in-plane carbon diffusion at 600 °C. Transformation of the surface conformation was monitored with bimodal atomic force microscopy at the atomic scale and was corroborated with core-level X-ray photoelectron spectroscopy. A strong C═O···H—C hydrogen bonding involving the quinone moiety plays a key role in graphene growth, whereas conventional pentacene simply desorbs from the substrate during the same process. The most significant achievement of this proposed technique is obtaining graphene a couple of hundred degrees lower than standard techniques. Intrinsic defects due to carbon deficiency and the defects intentionally introduced by the microscope tip were also investigated with atomic-scale imaging.

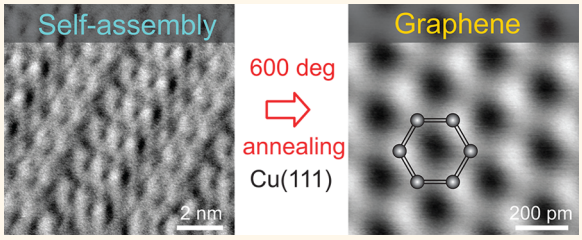

KEYWORDS: graphene · self-assembly · polymerization · bimodal AFM · XPS

Ever since its first isolation achieved by mechanical exfoliation from a bulk graphite crystal,[1] graphene has attracted tremendous scientific interest. Graphene not only possesses unusual electronic and mechanical properties such as high conductivity, quantum Hall effect and Berry's phase,[2] massless Dirac fermions,[3] and an elastic modulus of 1 TPa[4] but also offers unique technological applications such as gas sensors,[5] quantum computing elements, high-frequency transistors,[6,7] and terahertz oscillators. Fabrication techniques are of central importance for harnessing properties of graphene in an optimum way. Considering growth on metals, two common ways can be described.[8−10] The first way is *via* decomposition of hydrocarbons on metal surfaces with sufficient catalytic activity (*i.e.*, platinum) and is classified as chemical vapor deposition (CVD). Among metal substrates, a polycrystalline Cu substrate (Cu foil) is the most attractive due to low-cost and large-scale production.[11] Single-crystalline Cu substrates were also used in the literature for the CVD growth,[12,13] where high-temperatures around 1000 °C (very close to the melting point of Cu) were deemed necessary to form graphene in order to have a delicate balance between the sticking rate of hydrocarbon precursors and the dehydrogenation probability. The second pathway involves metal substrates with high carbon solubility at high temperatures (*i.e.*, nickel), from which carbon precipitates to the surface during cool-down, leading to crystallization of the pure graphene phase. In most cases, temperatures above 700 °C are considered a prerequisite, and annealing at lower temperatures typically results in amorphous and/or poorly crystalline carbon films.[14] Such high temperatures are undesirable for economical and environmental reasons; thus lowering the formation temperature is essential.

Here, we present a simple yet elegant solution for growing graphene on Cu(111) *via* a thermal polymerization of a self-assembled film of 6,13-pentacenequinone (PQ, $C_{22}H_{12}O_2$) molecules. Strong interaction of the carbonyl oxygen atom in a quinone moiety with the surface can prevent its desorption during annealing at 190 °C, enabling strong hydrogen bonding

* Address correspondence to shigeki.kawai@unibas.ch.

Received for review February 21, 2014 and accepted May 29, 2014.

Published online May 29, 2014
10.1021/nn501047v

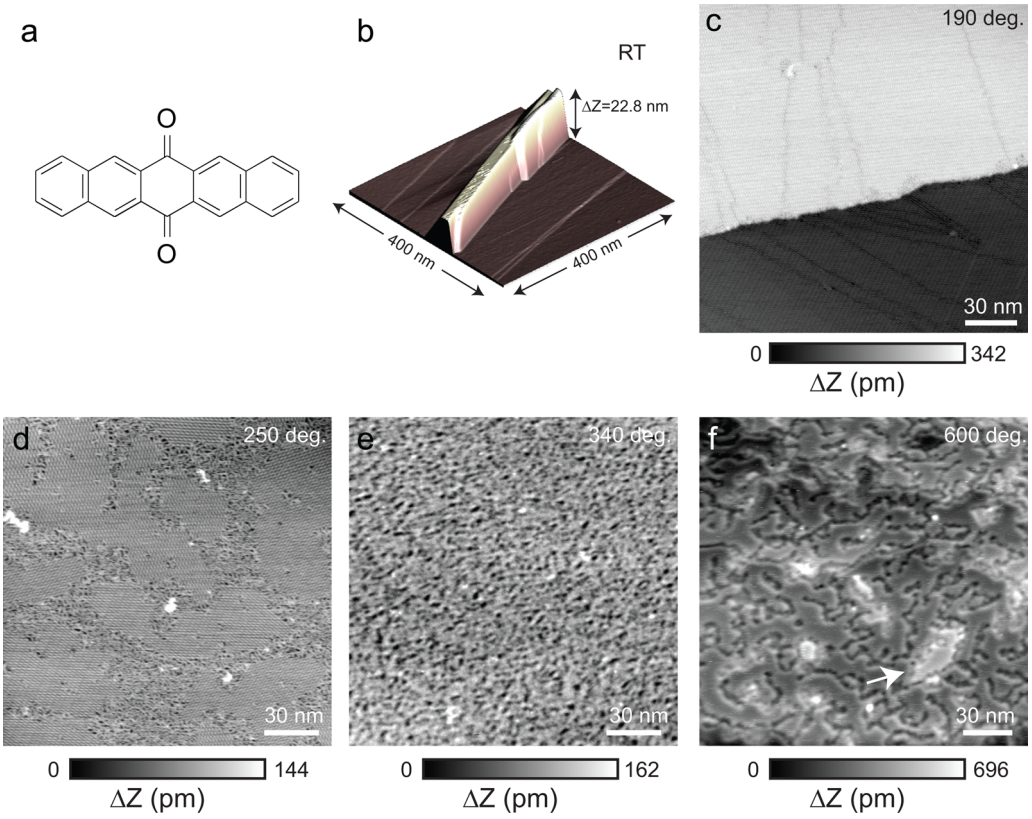

Figure 1. (a) Chemical structure of the PQ molecule. (b) Three-dimensional topographic view of as-deposited PQ molecules on a Cu(111) surface forming needle-like multiple layers. Topographic images obtained after different annealing steps at (c) 190 °C, (d) 250 °C, (e) 340 °C, and (f) 600 °C. Measurement parameters: A_{first} = 10 nm and Δf_{first} = −3.3 Hz in (b), A_{second} = 1.0 nm and Δf_{second} = −9.0 Hz in (c), A_{second} = 1.0 nm and Δf_{second} = −13.0 Hz in (d), A_{second} = 1.0 nm and Δf_{second} = −15.0 Hz in (e), and A_{first} = 2.0 nm and Δf_{first} = −12.0 Hz in (f).

between oxygen and hydrogen of a neighboring molecule. Deoxygenation, dehydrogenation, and in-plane carbon diffusion processes taking place during annealing at higher temperatures lead to covalent bonding between adjacent molecules. Consequently, the total molecular mass becomes large enough to inhibit desorption during annealing at elevated temperatures, eventually forming single-layer graphene graphene on Cu(111). Contrary to the standard CVD procedure, a lower formation temperature (600 °C) appeared to be sufficient.

RESULTS AND DISCUSSION

Transformation from a Self-Assembled Molecular Layer to Flat Films. Here, we show large-scale PQ structures on Cu(111) after each individual step. PQ molecules (Figure 1a) were *in situ* evaporated from a crucible of a Knudsen cell at 110 °C in ultrahigh vacuum (UHV) while the substrate was kept at room temperature (RT). UHV conditions were maintained during sample transfer and imaging. Figure 1b shows the topography of the as-deposited molecules obtained by noncontact atomic force microscopy (AFM) in the constant frequency mode at RT.[15] In contrast to pentacene ($C_{22}H_{14}$) molecules, which assemble in a layer-by-layer bulk structure in a standing-packing manner,[16] a needle-like structure was formed on top of the first PQ molecular layer, in which PQ molecules lie flat on the Cu(111) surface. This observation is in good agreement with the previous macroscopic measurements performed by Salzmann *et al.*,[17] and the mechanism to form the different assembly is related to the different electrostatic potential of PQ from pentacene due to the presence of a quinone moiety.[18] PQ molecules in the bulk crystal configuration were desorbed from the substrate by annealing at 190 °C. Although this temperature is much higher than the sublimation temperature of PQ molecules in the crucible (~110 °C), strong chemisorption on Cu(111) anchored PQ molecules in the first layer to the substrate, leaving a monolayer film behind, and thus the amount of deposited molecules in the initial step did not require high accuracy. The quality of the self-assembled molecular film also improved drastically after this thermal treatment, and the domain sizes became larger than 50 nm. Since the surface was no longer corrugated, small-amplitude operation with the second flexural mode of the cantilever was hereafter used to improve the spatial resolution in AFM topography images,[19,20] except for Figure 1d. Figure 1c shows the monolayer film with a domain size of up to 60 nm × 100 nm. The conformation of the self-assembly is in agreement with

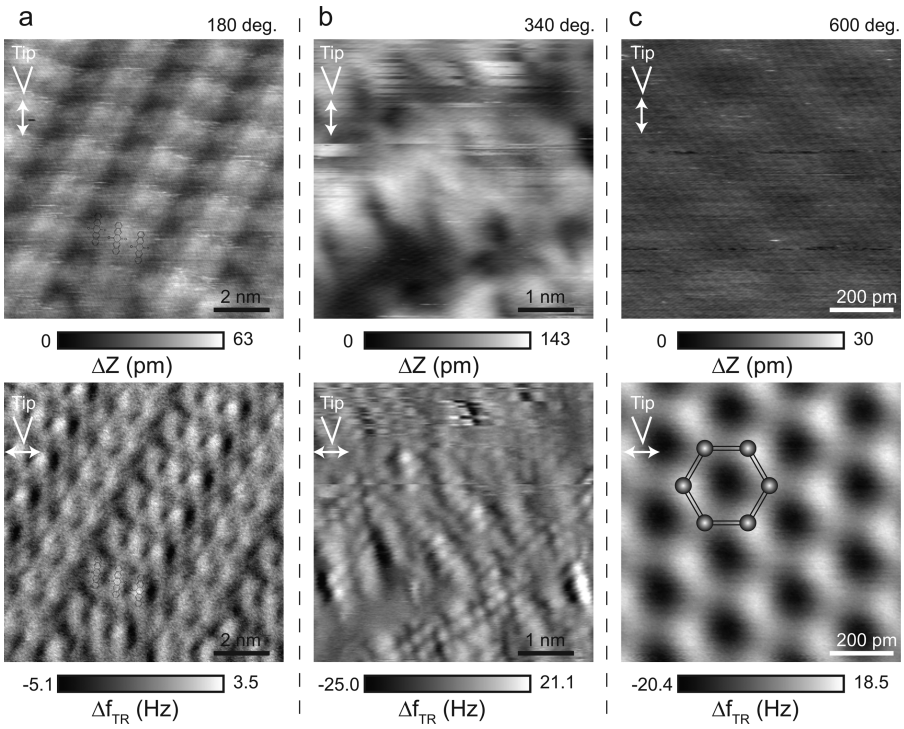

Figure 2. (a) Topographic (upper panel) and high-resolution Δf_{TR} maps (lower panel) of the self-assembled PQ film, (b) partially polymerized film, and (c) graphene. Measurement parameters: $\Delta f_{second} = -22.5$ Hz, $A_{second} = 1.0$ nm, and $A_{TR} = 30$ pm in (a), $\Delta f_{second} = -37.0$ Hz, $A_{second} = 1.0$ nm, and $A_{TR} = 30$ pm in (b), $\Delta f_{second} = -240$ Hz $A_{second} = 500$ pm, and $A_{TR} = 30$ pm in (c).

the previous scanning tunneling microscopy (STM) study,[21] as the carbonyl oxygen atom in the quinone moiety and a hydrogen atom of the adjacent molecule interacted in terms of strong C═O···H−C bonding on the surface.[18]

Disordered zones started to appear at domain boundaries of the self-assembled film after annealing at 250 °C (Figure 1d), suggesting that the first chemical reaction of molecules on Cu(111) took place. An activation energy is surmounted around this temperature, leading to a catalytic reaction between the carbonyl oxygen atom and a hydrogen atom from the adjacent molecule as a result of their affinity to each other, which was also shown to prevail in the conformation prior to this step. Combining with residual hydrogen in the UHV chamber, water molecules were likely to be formed and then released to the vacuum during this step. The binding energy of PQ molecules in the ordered zones to the Cu(111) substrate was high enough for them to remain attached to the surface at 250 °C. This is not a necessity for the disordered zones, since PQ molecules cannot be desorbed anymore even at higher temperatures once polymerization starts. At 340 °C, the self-assembled structure had completely vanished, and a single disordered hydrocarbon polymer monolayer was obtained (Figure 1e). The temperature of the final annealing step was 600 °C, at which only flat islands separated by grooves were observed (Figure 1f). Furthermore, some of the islands indicated by an arrow are about 200 pm higher than the rest, associated with the second layer. It is noteworthy to mention here that dehydrogenation presumably had already started at temperatures lower than 600 °C;[22] however no significant effect had been observed since the carbon mobility was limited at these temperatures.

Atomic-Scale Measurements. Transition of the structure at atomic scale was studied by high-resolution imaging. In order to achieve high-resolution images of the films, we used the recently developed bimodal AFM technique,[23] in which two resonance modes of the cantilever were simultaneously employed.[24,25] In this technique, the frequency shift of the vertical oscillation was used to control the tip−sample Z distance (topographic image), and that of the torsional oscillation Δf_{TR} ensured high-resolution imaging.[26,27] Figure 2a shows the topographic image of the initial self-assembled PQ film on the Cu(111) surface. The inset shows a plausible conformation, where the molecules self-assemble in such a way as to form the C═O···H hydrogen bonds with the adjacent molecules. The conformation of the PQ assembly is very similar to that previously reported on MoS_2 by Strohmaier *et al.*[21] In addition, we observed the superstructure, in which characteristic bright zones run in every three molecules. Since this feature was observed with a different measurement set point, it cannot be related to an imaging artifact. Presumably, the strong chemisorption of the molecules to the Cu substrate and its resultant commensurability induce this superstructure.

The lower panel shows the corresponding Δf_{TR} map. Since the direction of the tip apex movement by the torsional vibration of the cantilever is along the X direction (inset), the Δf_{TR} map is related to the lateral force gradient, which is the second derivative of the potential map along the X direction. The site-independent tip−sample interaction causes no lateral force gradient, so that the detected Δf_{TR} is only related to the site-dependent interaction. On an atomically flat surface, the short-range tip−sample interaction is responsible for the contrast and atoms are usually observed as more positive Δf_{TR} sites. However, on molecular films, middle-range tip−molecular interactions can also contribute to Δf_{TR}. This imaging mechanism makes the interpretation of the contrast more complicated compared to a conventional topography obtained by the vertical tip−sample interaction. Furthermore, two oxygen atoms in the PQ molecule bind to the Cu substrate, resulting in a V-shaped bending configuration of the molecule such that both longitudinal ends reside facing up. These complexities induced the peculiar contrast shown in the lower panel of Figure 2a; nonetheless, clear periodic patterns with submolecular resolution are clear evidence of the presence of a highly ordered molecular film. Annealing at 250 °C induced partial polymerization of PQ molecules and introduced a flake-like structure in the topography and some new patterns with the periodicity of the lattice parameter of graphene in the Δf_{TR} map (Figure 2b), but without any long-range order (domain size less than a few nanometers). The remaining line structures are most probably related to PQ molecules, which were not yet covalently bonded to each other.

After annealing at 600 °C, the topographic image in the island becomes very flat (<30 pm), all of the PQ molecules were perfectly polymerized, and graphene was eventually formed (Figure 2c). All carbon atoms can be clearly resolved in such a way that the atomic sites reveal bright contrast, whereas the hollow sites are dark. Such contrast is observed only in the Δf_{TR} map. Assuming Arrhenius diffusion kinetics for the carbon atoms in the disordered polymer, 600 °C appears to be the necessary temperature to surmount the potential energy barrier. In a recent study, such diffusion for graphene nanoribbon formation on a weaker catalytic surface of Au(111) was observed at 400 °C.[28] In the present method, the surface still consists of a disordered polymer at this temperature. This might be due to the fact that closing defect sites in two-dimensional graphene requires a higher temperature. Moreover, since graphene has a larger carbon density than the PQ molecular layer, the insufficient feedstock leads to the formation of grooves between the graphene layers as shown in Figure 1f. It is also worth mentioning the complex imaging mechanism of the graphite surface. Since the carbon atom is rather small, the hollow is observed as the convex site with a large tip−sample separation. On the contrary, when the tip comes closer to the sample surface, all carbon atoms can be observed.[29−32] In fact, the maxima in the topography do not correspond to the hollow site. Despite that the reactivity of the tip also changes the atomic-scale contrast,[33] the interpretation of the contrasts can still be rationalized. In the Δf_{TR} map, a three-fold symmetric feature is observed, which is typical for graphite that has α and β sites.[34,35] However, since we are observing single-layer graphene, such an effect can be excluded. This is most probably due to the fact that the lattice distance of Cu is close to that of graphene, so that the interfacial interaction induces the three-fold symmetric feature. In fact, a previous study with STM shows a similar three-fold symmetric feature,[12] but it can also be due to an imaging artifact, for instance, the tip apex oscillating nonperfectly parallel to the surface.

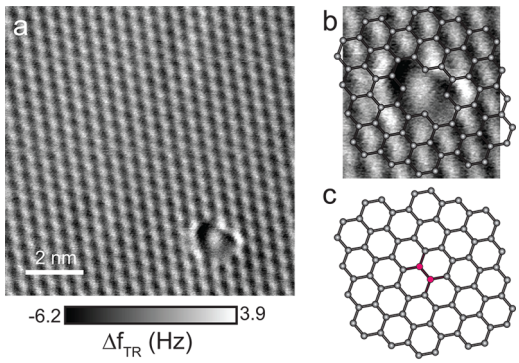

Figure 3. (a) High-resolution Δf_{TR} map of graphene with a defect. (b) Magnified image around the defect and (c) its chemical structure. The red dots indicate the missing carbon atoms. Measurement parameters: A_{second} = 1.0 nm, Δf_{second} = −90.0 Hz, f_{second} = 1 041 450 Hz, Q_{second} = 4895, A_{TR} = 30 pm, f_{TR} = 1 536 483 Hz, and Q_{TR} = 80 776.

Atomic-Scale Defect and Deformation. Compared to standard CVD, the substrate temperature at the formation temperature of graphene in this technique is around 400 °C lower; hence there is limited in-plane carbon diffusion. Together with the fact that monolayer PQ has a lower carbon density than graphene, this results in a large defect density (*e.g.*, grooves in Figure 2f). Figure 3a shows an example of a carbon deficiency defect in the graphene sheet with hollow sites appearing as bright contrast. Local protrusions in the contrast due to the medium-ranged corrugation of the potential modulated by the defect can be observed in the vicinity of the defect site. Figure 3b presents the magnified image around the defect, clearly showing four missing hollow sites. Since hollow sites appear in the signal as a result of carbon ring−tip interactions, we suggest that two carbon atoms were missing and the connecting carbons were terminated by hydrogen atoms (Figure 3c).

The tip was intentionally contacted into the sample surface, expecting to deform the Cu substrate below graphene due to its high compliance. As shown in the topographic image after the tip contact (Figure 4a), an

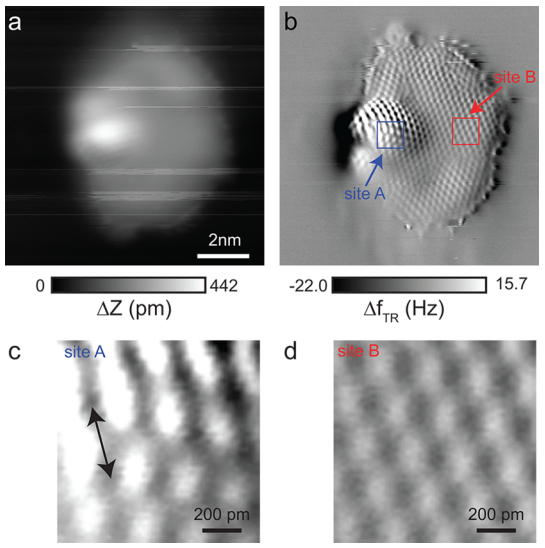

Figure 4. (a) AFM topography and (b) high-resolution Δf_{TR} maps of graphene deformed by the tip. Magnified images of (c) site A and (d) site B that are indicated in (b). Measurement parameters: A_{second} = 500 pm, Δf_{second} = −130.0 Hz, f_{second} = 1 041 450 Hz, Q_{second} = 4895, A_{TR} = 30 pm, f_{TR} = 1 536 483 Hz, and Q_{TR} = 80 776.

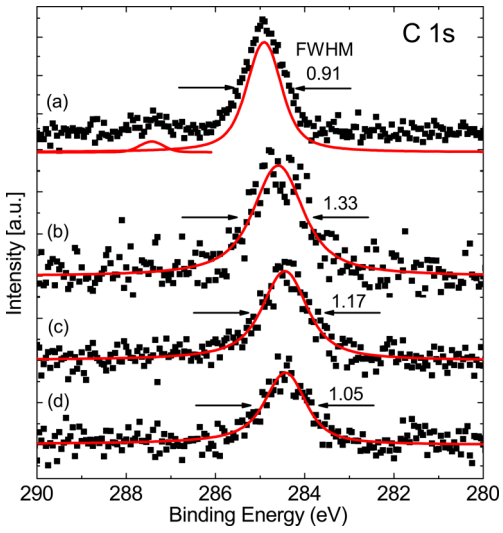

Figure 5. Core level C 1s spectra acquired during transformation of the PQ deposit into graphene: (a) as-deposited multilayer PQ molecules; (b) monolayer rearrangement of PQ deposit after annealing at 170 °C; (c) polymerization after annealing at 370 °C; (d) graphene formation after annealing at 600 °C. Dots are the measured data after background subtraction, and the solid red lines are the fitted curves.

inhomogeneously subnanometer corrugated surface was achieved. The corresponding Δf_{TR} map shows a more detailed structure and allows us to make the following observations: (1) The tip−sample separation, which is controlled by the constant vertical frequency shift, varies by the modulation of the short- and long-range interactions and becomes smaller at the protruded area. Therefore, only the corrugated area can be atomically resolved. (2) Graphene seems atomically damaged at the edge of the round shape and especially on the right-hand side of the protruded surface. (3) Figure 4c and d have the same real dimensions and show the magnified images at sites A and B. The lattice spacing in Figure 4c in the direction indicated with an arrow is approximately 15% larger than that of Figure 4d. This extension suggests that the graphene sheet conformed to the corrugation of Cu; thus carbon bonds were stretched. In contrast, at site B, the deformed substrate was rather flat and the intrinsic lattice geometry of graphene remained intact. This observation provides firsthand evidence that graphene can be locally deformed in the tensile direction without rupture. The magnitude of the strain was still less than the critical value for the rupture (∼20%), calculated with density-functional theory by Topsakal and Ciraci.[36] It is also noteworthy to mention that the typical Moiré patterns, caused by the lattice mismatch between graphene and the supporting substrate, is a manifestation of compressive stress along the graphene sheet, meaning that it is in the direction opposite of the current observation.

XPS Measurements. The transformation from deposited PQ molecules to graphene was monitored with X-ray photoelectron spectroscopy (XPS) measurements, which lent support to our claims by providing the chemical states. Before the measurement, the cleanliness of the Cu substrate was checked with wide-range XPS spectra from 0 to 1000 eV. Since no other peak than those related to copper was detected, the Cu substrate was sufficiently clean. Figure 5 shows the core level C 1s spectra acquired after each thermal treatment step. In Figure 5a, the spectrum consists of two peaks: the peak at higher binding energies (∼287.5 eV) assigned to the carbonyl carbon (C═O) and the main peak at lower binding energies assigned to aromatic carbon bonds (284.9 eV). After the first annealing step at 170 °C, three differences associated with the monolayer arrangement of PQ molecules on the Cu(111) surface can be observed: (1) The relative intensity of the C 1s with respect to Cu 2p dropped by a factor of around 2.5; (2) the binding energy of the main C 1s peak is shifted around −0.3 eV due to the effective metal screening[37,38](Figure 5b); (3) the main peak appeared broader, which is probably a convolution of two chemically inequivalent peaks as in the case of pentacene,[38,39] where strong chemisorption involving a hybridization of molecular orbitals and metal states has been suggested.[40] Because of the low intensity, the signal-to-noise ratio of the C═O peak became quite low, although some features at the higher binding energy tail of the main peak still exist.

Subsequent thermal treatments at higher temperatures (Figure 5c,d) resulted in narrowing of the main peak, suggesting that carbon started to be present only in one distinct chemical environment. At these stages, the higher binding energy tail of the main peak appeared completely flat, suggesting the suppression

of the C═O peak related to oxygen-free polymerization. Graphene is known to be weakly physisorbed on the Cu(111) surface because the Cu 3d states are fully occupied and pushed down from the Fermi level.[12] Due to this reason, the main peak appeared at the same binding energy (284.4 eV) and asymmetry parameter (0.11) as those of a reference graphite sample at the final stage of the growth.[41]

CONCLUSION

In summary, we fabricated graphene from a deposit of pentacenequinone molecules on Cu(111) *via* a multistep thermal treatment involving single-layer self-assembly, polymerization and in-plane carbon diffusion steps, the latter forming single-layer graphene at 600 °C. The crucial point is using a molecule with a quinone moiety that ensures stronger binding to the surface and at a later stage covalently binds to adjacent molecules by producing H_2O molecules, consequently increasing the apparent molecular mass to avoid the desorption from the substrate before dehydrogenation at higher annealing temperatures. In fact, the conventional pentacene simply desorbs from the Cu(111) surface before the polymerization starts. Furthermore, the density of defects is rather high at the moment. This is due to the low diffusion of the carbon atom in plane. Attempts to improve the quality by longer and/or higher temperature annealing and comparing its quality with the graphene grown by standard chemical vapor deposition technique are highly required. Since the first step in the presented method exploits the well-established self-assembly mechanism, controllability of graphene chemistry, *viz.*, boron- or nitrogen-doped graphene from molecules (or admixtures) containing these two elements, is a possible prospect. This technique also has the advantage of employing lower temperatures over standard CVD and, therefore, can be employed in graphene formation on patterned nanometer Cu structures obtained by nanostencil lithography.[42]

METHODS

In this study, AFM and XPS measurements were separately performed in identical UHV conditions.

AFM Measurements. All AFM measurements were performed with our custom-built AFM operating in an UHV at RT.[43] A commercially available Si cantilever (Nanosensor NCL-PPP) was used as the force sensor, which was annealed at 120 °C, and its tip was subsequently cleaned by Ar^+ sputtering (680 eV and 90 s). The measurements were performed either in the conventional constant frequency mode with the first flexural resonance, in small-amplitude mode with the second flexural resonance, or in bimodal operation mode[23−27] using the second flexural and first torsional resonance modes by simultaneously oscillating the cantilever vertically and laterally. Frequency shifts were detected with two sets of digital phase-locked loops (Nanonis: dual-OCH4). The resonance frequencies of the flexural and torsional modes were $f_{ver} \approx 1$ MHz and $f_{TR} \approx 1.5$ MHz, respectively. Recorded data were analyzed using the WSxM software.[44]

XPS Measurements. These were performed in UHV with a VG ESCALAB 210 spectrometer using monochromatic Al Kα radiation (1486.6 eV) with an energy resolution of 0.5 at 20 eV analyzer pass energy. The base pressure in the chamber was around 1×10^{-9} mbar during acquisition. Normal electron escape angle and a step size of 0.05 eV were used. The Au $4f_{7/2}$ was fixed to a binding energy of 84 eV with respect to Fermi level for binding energy calibration.

Sample Preparation. A clean Cu(111) surface was obtained by several cycles of standard Ar^+ sputtering (3×10^{-6} mbar, 1 keV, and 15 min) and annealing (500 °C and 15 min). PQ molecules (Sigma-Aldrich, nominal purity = 99%) were deposited on the Cu(111) substrate from a crucible of a Knudsen cell, resistively heated at ∼110 °C after being degassed for several hours at ∼95 °C. The temperature of the substrate was kept at RT during deposition, while the deposition rate was around 1.2 Å/min. The thermal treatment steps at various temperatures mentioned in the main text were performed for 15 min, while measured with a pyrometer. After the sample had cooled to RT, it was transferred *in situ* to the analysis chambers, in which the AFM and XPS measurements were separately performed.

Conflict of Interest: The authors declare no competing financial interest.

Acknowledgment. This work was supported by the Swiss National Science Foundation, the Swiss Federal Office of Energy and the Federal Office for Education and Science, the National Center of Competence in Research on Nanoscale Science (NCCR-Nano), by COST Action MP1303, and by the Japan Science and Technology Agency (JST) 'Precursory Research for Embryonic Science and Technology (PRESTO)' as part of the 'Molecular Technology and Creation of New Function' project.

REFERENCES AND NOTES

1. Novoselov, K. S.; Geim, A. K.; Morozov, S. V.; Jiang, D.; Zhang, Y.; Dubonos, S. V.; Grigorieva, I. V.; Firsov, A. A. Electric Field Effect in Atomically Thin Carbon Films. *Science* **2004**, *306*, 666–669.
2. Zhang, Y.; Tan, Y.-W.; Stormer, H. L.; Kim, P. Experimental Observation of the Quantum Hall Effect and Berry's Phase in Graphene. *Nature* **2005**, *438*, 201–204.
3. Zhou, S. Y.; Gweon, G.-H.; Graf, J.; Fedorov, A. V.; Spataru, C. D.; Diehl, R. D.; Kopelevich, Y.; Lee, D.-H.; Louie, S. G.; Lanzara, A. First Direct Observation of Dirac Fermions in Graphite. *Nat. Phys.* **2006**, *2*, 595–599.
4. Lee, C.; Wei, X.; Kysar, J. W.; Hone, J. Measurement of the Elastic Properties and Intrinsic Strength of Monolayer Graphene. *Science* **2008**, *321*, 385–388.
5. Schedin, F.; Geim, A. K.; Morozov, S. V.; Hill, E. W.; Blake, P.; Katsnelson, M. I.; Novoselov, K. S. Detection of Individual Gas Molecules Adsorbed on Graphene. *Nat. Mater.* **2007**, *6*, 652–655.
6. Lin, Y.-M.; Jenkins, K. A.; Valdes-Garcia, A.; Small, J. P.; Farmer, D. B.; Avouris, P. Operation of Graphene Transistors at Gigahertz Frequencies. *Nano Lett.* **2009**, *9*, 422–426.
7. Lin, Y.-M.; Dimitrakopoulos, C.; Jenkins, K. A.; Farmer, D. B.; Chiu, H.-Y.; Grill, A.; Avouris, Ph. 100-GHz Transistors from Wafer-Scale Epitaxial Graphene. *Science* **2010**, *327*, 662.
8. Wintterlin, J.; Bocquet, M.-L. Graphene on Metal Surfaces. *Surf. Sci.* **2009**, *603*, 1841–1852.
9. Bartelt, N. C.; McCarty, K. F. Graphene Growth on Metal Surfaces. *MRS Bull.* **2012**, *37*, 1158–1165.
10. Iski, E. V.; Yitamben, E. N.; Gao, L.; Guisinger, N. P. Graphene at the Atomic-Scale: Synthesis, Characterization, and Modification. *Adv. Funct. Mater.* **2013**, *23*, 2554–2564.
11. Bae, S.; Kim, H.; Lee, Y.; Xu, X.; Park, J.-S.; Zheng, Y.; Balakrishnan, J.; Lei, T.; Kim, H. R.; Song, Y. I.; *et al.* Roll-to-Roll Production of 30-in. Graphene Films for Transparent Electrodes. *Nat. Nanotechnol.* **2010**, *5*, 574–578.

12. Gao, L.; Guest, J. R.; Guisinger, N. P. Epitaxial Graphene on Cu(111). *Nano Lett.* **2010**, *10*, 3512–3516.
13. Rasool, H. I.; Song, E. B.; Mecklenburg, M.; Regan, B. C.; Wang, K. L.; Weiller, B. H.; Gimzewski, J. K. Atomic-Scale Characterization of Graphene Grown on Copper (100) Single Crystals. *J. Am. Chem. Soc.* **2011**, *133*, 12536–12543.
14. Wofford, J. M.; Nie, S.; McCarty, K. F.; Bartelt, N. C.; Dubon, O. D. Graphene Islands on Cu Foils: The Interplay between Shape, Orientation, and Defects. *Nano Lett.* **2010**, *10*, 4890–4896.
15. Albrecht, T. R.; Grütter, P.; Horne, D.; Rugar, D. Frequency Modulation Detection Using High-Q Cantilevers for Enhanced Force Microscope Sensitivity. *J. Appl. Phys.* **1991**, *69*, 668–673.
16. Kawai, S.; Pawlak, R.; Glatzel, T.; Meyer, E. Systematic Measurement of Pentacene Assembled on Cu(111) by Bimodal Dynamic Force Microscopy at Room Temperature. *Phys. Rev. B* **2011**, *84*, 085429.
17. Salzmann, I.; Opitz, R.; Rogaschewski, S.; Rabe, J. P.; Koch, N.; Nickel, B. Phase Separation in Vacuum Codeposited Pentacene/6,13-Pentacenequinone Thin Films. *Phys. Rev. B* **2007**, *75*, 174108.
18. Käfer, D.; Helou, M. E.; Gemel, C.; Witte, G. Packing of Planar Organic Molecules: Interplay of van der Waals and Electrostatic Interaction. *Cryst. Growth Des.* **2008**, *8*, 3053–3057.
19. Kawai, S.; Kitamura, S.; Kobayashi, D.; Meguro, S.; Kawakatsu, H. An Ultrasmall Amplitude Operation of Dynamic Force Microscopy with Second Flexural Mode. *Appl. Phys. Lett.* **2005**, *86*, 193107.
20. Kawai, S.; Rose, F.; Ishii, T.; Kawakatsu, H. Atomically Resolved Observation of the Quenched Si(111) Surface with Small Amplitude Dynamic Force Microscopy. *J. Appl. Phys.* **2006**, *99*, 104312.
21. Strohmaier, R.; Petersen, J.; Gompf, B.; Eisenmenger, W. A Systematic STM Study of Planar Aromatic Molecules on Inorganic Substrates: I. Submolecular Image Contrast. *Surf. Sci.* **1998**, *418*, 91–104.
22. Cai, J.; Ruffieux, P.; Jaafar, R.; Bieri, M.; Braun, T.; Blankenburg, S.; Muoth, M.; Seitsonen, A.-P.; Saleh, M.; Feng, X.; *et al.* Atomically Precise Bottom-up Fabrication of Graphene Nanoribbons. *Nature* **2010**, *466*, 470.
23. Kawai, S.; Glatzel, T.; Koch, S.; Such, B.; Baratoff, A.; Meyer, E. Systematic Achievement of Improved Atomic-Scale Contrast *via* Bimodal Dynamic Force Microscopy. *Phys. Rev. Lett.* **2009**, *103*, 220801.
24. Martinez, N. F.; Patil, S.; Lozano, J. R.; García, R. Enhanced Compositional Sensitivity in Atomic Force Microscopy by the Excitation of the First Two Flexural Modes. *Appl. Phys. Lett.* **2006**, *89*, 153115.
25. Lozano, J. R.; García, R. Theory of Multifrequency Atomic Force Microscopy. *Phys. Rev. Lett.* **2008**, *100*, 076102.
26. Kawai, S.; Glatzel, T.; Koch, S.; Such, B.; Baratoff, A.; Meyer, E. Ultrasensitive Detection of Lateral Atomic-Scale Interactions on Graphite (0001) *via* Bimodal Dynamic Force Measurements. *Phys. Rev. B* **2010**, *81*, 085420.
27. Kawai, S.; Federici Canova, F.; Glatzel, T.; Hynninen, T.; Meyer, E.; Foster, A. S. Measuring Electric Field Induced Subpicometer Displacement of Step Edge Ions. *Phys. Rev. Lett.* **2012**, *109*, 146101.
28. van der Lit, J.; Boneschanscher, M. P.; Vanmaekelbergh, D.; Ijäs, M.; Uppstu, A.; Ervasti, M.; Harju, A.; Liljeroth, P.; Swart, I. Suppression of Electronvibron Coupling in Graphene Nanoribbons Contacted via a Single Atom. *Nat. Commun.* **2013**, *4*, 2023.
29. Allers, W.; Schwarz, A.; Schwarz, U. D.; Wiesendanger, R. Dynamic Scanning Force Microscopy at Low Temperatures on a van der Waals Surface: Graphite (0001). *Appl. Surf. Sci.* **1999**, *140*, 247.
30. Hölscher, H.; Allers, W.; Schwarz, U. D.; Schwarz, A.; Wiesendanger, R. Interpretation of "True Atomic Resolution" Images of Graphite (0001) in Noncontact Atomic Force Microscopy. *Phys. Rev. B* **2000**, *62*, 6967.
31. Hembacher, S.; Giessibl, F. J.; Mannhart, J.; Quate, C. F. Revealing the Hidden Atom in Graphite by Low-Temperature Atomic Force Microscopy. *Proc. Natl. Acad. Sci. U.S.A.* **2003**, *100*, 12539.
32. Ondrácek, M.; Pou, P.; Rozsíval, V.; González, C.; Jelínek, P.; Pérez, R. Forces and Currents in Carbon Nanostructures: Are We Imaging Atoms? *Phys. Rev. Lett.* **2011**, *106*, 176101.
33. Boneschanscher, M. P.; van der Lit, J.; Sun, Z.; Swart, I.; Liljeroth, P.; Vanmaekelbergh, D. Quantitative Atomic Resolution Force Imaging on Epitaxial Graphene with Reactive and Nonreactive AFM Probes. *ACS Nano* **2012**, *6*, 10216–10221.
34. Binnig, G.; Garber, C.; Stoll, E.; Albrecht, T. R.; Quate, C. F. Atomic Resolution with Atomic Force Microscope. *Europhys. Lett.* **1987**, *3*, 1281–1286.
35. Kawai, S.; Kawakatsu, H. Surface-relaxation-induced Giant Corrugation on Graphite (0001). *Phys. Rev. B* **2009**, *79*, 115440.
36. Topsakal, M.; Ciraci, S. Elastic and Plastic Deformation of Graphene, Silicene, and Boron Nitride Honeycomb Nanoribbons under Uniaxial Tension: A First-Principles Density-Functional Theory Study. *Phys. Rev. B* **2010**, *81*, 024107.
37. Gumhalter, B.; Newns, D. M. Dynamic Screening in Photoemission from Adsorbed Species. *Phys. Lett. A* **1975**, *53*, 137–138.
38. McDonald, O.; Cafolla, A. A.; Li, Z.; Hughes, G. Synchrotron Photoemission Studies of Pentacene Films on Cu(1 1 0). *Surf. Sci.* **2006**, *600*, 1909–1916.
39. Koch, N.; Gerlach, A.; Duhm, S.; Glowatzki, H.; Heimel, G.; Vollmer, A.; Sakamoto, Y.; Suzuki, T.; Zegenhagen, J.; Rabe, J. P.; *et al.* Adsorption-Induced Intramolecular Dipole: Correlating Molecular Conformation and Interface Electronic Structure. *J. Am. Chem. Soc.* **2008**, *130*, 7300–7304.
40. Ferretti, A.; Baldacchini, C.; Calzolari, A.; Di Felice, R.; Ruini, A.; Molinari, E.; Betti, M. Mixing of Electronic States in Pentacene Adsorption on Copper. *Phys. Rev. Lett.* **2007**, *99*, 046802.
41. Eren, B.; Hug, D.; Marot, L.; Pawlak, R.; Kisiel, M.; Steiner, R.; Zumbuehl, D. M.; Meyer, E. Pure Hydrogen Low-Temperature Plasma Exposure of HOPG and Graphene: Graphane Formation? *Beilstein J. Nanotechnol.* **2012**, *3*, 852–859.
42. Gross, L.; Schlittler, R. R.; Meyer, G.; Fendt, L.-A.; Diederich, F.; Glatzel, T.; Kawai, S.; Koch, S.; Meyer, E. Contacting Self-ordered Molecular Wires by Nanostencil Lithography. *J. Vac. Sci. Technol. B* **2010**, *28*, C4D34.
43. Howald, L.; Meyer, E.; Lüthi, R.; Haefke, H.; Overney, R.; Rudin, H.; Güntherodt, H.-J. Multifunctional Probe Microscope for Facile Operation in Ultrahigh Vacuum. *Appl. Phys. Lett.* **1993**, *63*, 117–119.
44. Horcas, I.; Fernandez, R.; Gomez-Rodriguez, J.; Colchero, J.; Gomez-Herrero, J.; Baro, A. WSXM: A Software for Scanning Probe Microscopy and a Tool for Nanotechnology. *Rev. Sci. Instrum.* **2007**, *78*, 013705.